Multi-target-based screening of phytochemicals found in aerial parts of *Heliotropium indicum* L. for identification of potential anti-urolithiatic agents using simulation methods

Vivek Kumar
MDU, Rohtak, India
Pawan Gupta
pawan.gupta@svkm.ac.in

Department of Pharmaceutical Chemistry, Shri Vile Parle Kelavani Mandal's Institute of Pharmacy, Dhule, Maharashtra, India-424001
https://orcid.org/0000-0001-7201-1356
Vishnu Sharma
Department of Pharmacoinformatics, National Institute of Pharmaceutical Education and Research (NIPER), Mohali, Punjab, India-160062
Anju Dhiman
MDU, Rohtak, India

Research Article

Keywords: Urolithiasis, Phytochemicals, Muti-targets-based virtual screening, Docking, Molecular dynamic simulation

Posted Date: September 25th, 2024

DOI: https://doi.org/10.21203/rs.3.rs-5144782/v1

Additional Declarations: The authors declare no competing interests.

Abstract

BackGround:

Heliotropium indicum Linn., a plant also known as 'Indian heliotrope,' is found in tropical and temperate regions of the world, and throughout India. This plant exhibits varieties of therapeutic effects like anti-inflammatory, anti-bacterial, anti-fertility, anti-nociceptive, and anti-tumor activities. In addition, the *Heliotropium indicum* L. plant have been reported to have therapeutic effects in kidney stone or urolithiasis. But it is not reported to date which phytochemicals are responsible for this activity. The current studies deal with multi-targets-based virtual screening for identification of the phytochemicals found in *Heliotropium indicum*L. aerial parts against different targets and understanding their binding potential and pharmacokinetic profiles. The multitarget based virtual screening of phytochemical found in aerial part of *Heliotropium indicum* L. was performed against different anti-urolithiatic targets using molecular docking and molecular dynamic simulations.

Results

From the molecular docking-based screening, it was found that phytochemicals *Pestalamide B*, *Rapanone*, and *Supinine* possess had excellent binding modes against almost all the different targets selected for urolithiasis activities. Further validation in molecular dynamic simulations studies, these phytochemicals (Pestalamide B, Rapanone, Supinine) were supported docking results in term of stability and binding properties.

Conclusion:

Therefore, these phytochemicals (Pestalamide B, Rapanone, Supinine) from *Heliotropium indicum* L. aerial parts were found to have high potential most of the anti-urolithiatic targets as compared to other phytochemicals. However, these need to be proved experimentally. The results of the current studies can be exploited further for designing and discovering new anti-urolithiasis agents for the treatment of kidney stone/urolithiasis.

1. Background

Urolithiasis (Kidney stone in the urinary tract) is a multifarious process caused by an imbalance between stone inhibitors and promoter factors in kidneys [1].The precipitation of oxalate and phosphate salts is occurs in the urinary tract which can obstruct the urethra that results in renal colic, haematuria, pyuria, dysuria, and oliguria [2, 3]. The formation of these stones blocks the flow of urine resulting in pain [4, 5]. In the past few years, the incidence of kidney stones has increased in both males and females may be due to the high dietary intake of minerals and proteins. In addition, the male sex hormone testosterone has been found an enhanced effect on kidney stone formation while the female sex hormone estrogen has been responsible for the prevention of kidney stone formation as it is keeping urine pH alkaline and increasing citrate levels in urine [6–9].The recurrence rate of this disease differs in males (70–80%) and in females (47–60%) [10].

Stone formation is a cascade of events including nucleation, growth, aggregation, and retention of crystals within the kidneys. In the first step of the formation of kidney stones, crystal nucleation begins with the formation of the nucleus (termed as nidus) from supersaturated urine retained inside the kidney [11, 12]. The crystals in urine are starting to stick together to form a small hard mass of the stone, this process is termed crystal growth. The next step is crystal aggregation, in which a small hard mass of a crystal in solution sticks together to form a larger stone. In this step, aggregation of preformed crystals or secondary nucleation of crystal on the matrix-coated surface occurs. The stone growth and aggregation processes are slow and require a longer time to get a bigger size and subsequent blocking and retention of stone in the renal tubules [13]. The crystal can get interacted and/or attach to the epithelial cells lining the renal tubule of lining which may lead to damage to the epithelial cells and produce tubule injury [14].

The aberration in the chemical composition of the urine is related to the chemical composition of kidney stones [15, 16]. 80% of urinary stones are predominantly contained calcium oxalate [17]. The majority of calcium oxalate is found in the form of calcium oxalate monohydrate (COM), and calcium oxalate dihydrate (COD), or a combination of both which accounts for greater than 60% [18]. However, the struvite stone (magnesium ammonium phosphate) is also commonly found in the upper urinary tract due to bacteria infection [19]. Other stones, like ammonium acid urate, monosodium urate monohydrate, uric acid anhydrous, uric acid mono, and dihydrate are also found [20, 21].

Oxidative stress is caused by the imbalance of antioxidant capacity and reactive oxygen species (ROS) production. The ROS is formed via the involvement of mitochondria and NADPH oxidase (especially in the kidney) [22].Under normal conditions, ROS found as a mediator of several signalling pathways including apoptosis, proliferation, and regulation of gene/transcription factor [22–24]. But, ROS also responsible for inducing oxidative stress which is critical for the formation of kidney stone/urolithiasis [22, 25]. It has been reported that oxidative stress increases the deposition of calcium oxalate crystals (kidney stones) [26, 27]. This oxidative stress causes injury to the renal epithelial cells and interacts with calcium oxalate crystals or oxalate ions is likely to enhance renal calculi formation [22, 23]. The increased oxidative stress causes ROS-induced cell injury, damage, and inflammation. The human body is having an antioxidant defensive mechanism which is used to scavenge the ROS and protect the body from the development of oxidative stress- mediated diseases including kidney stones. Therefore, the therapeutic intervention of antioxidants is helping to reduce oxidative stress/damage and crystal deposits [24]. Citrate is widely used as a key therapeutic agent for inhibiting kidney stones. Citrate is found in citrus as well as non-citrus fruits [28, 29]. Natural antioxidants like phenols and flavonoids were reported to mitigate free radical toxicity and alleviate stone formation in animal models as well as humans [30–33]. Therefore, phytochemicals with antioxidant activities could be useful in kidney stone prevention.

For the management of urolithiasis or kidney stones, several protein targets were reported [34]. Glycolate oxidase (GO) (PDB ID: 2RDT) [35, 36] is expressed in the liver and pancreas and localized in peroxisomes. The dietary glycolate directly or indirectly is converted by peroxisomal GO (EC 1.1.3.15) into glyoxylate to oxalate. So, the GO is responsible for the overproduction of oxalate from glyoxylate [35, 37]. The high concentration of oxalate is responsible for hyperoxaluria which leads to kidney stone formation. Moreover, the function of GO in glyoxylate production plays an important role in Primary hyperoxaluria

type 1 (PH1, a genetic disorder that leads to the formation of a high level of oxalate or hyperoxaluria) and oxalate mediates disorders [38, 39]. The inhibition of GO has been identified as a potential treatment for PH1 and oxalate mediate disorder scan be targeted to inhibit/stop oxalate formation [35, 37, 38]. In addition, the antioxidant enzymes have also been found to be significant for urolithiasis management by preventing oxidative damage and protective effect on kidney stones. Antioxidant enzymes prevent calcium oxalate retention which could be precipitated into kidney stones [30–34, 40, 41]. The antioxidant protein targets are glutathione-disulfide reductase (PDB ID: 1BWC[42]), glutathione-S-transferase(PDBID: 4MPG), superoxide dismutase (PDB ID: 1CB4 [43]) and glutathione peroxidase (PDB ID: 2WGR [44]).

The human calcium-sensing receptor (PDB ID: 5FBH[45]) is a G-coupled protein receptor responsible for calcium homeostasis in the body. The reduction in calcium-sensing receptor expression in the medulla of the kidney may lead to the formation of calculi. It may occur due to the imbalance in the excretion of water, calcium, and phosphate. This imbalance leads to calcium-phosphate precipitation and results in the formation of the stone [46]. Previous research has confirmed that this receptor is to be responsible for the formation of kidney stones [45, 47, 48].

In addition, matrix metalloproteinase (MMP)-9 (PDB ID: 4XCT[49]) and MMP2 (PDB ID: IHOV[50]) were also found to be important biomarkers in several kidney diseases[25, 51, 52]. Wu et al. reported that the inhibition of reactive oxygen species (ROS) production or the nuclear factor kappa-light chain-enhancer of activated B cell (NF-κB) pathway is significantly reduced calcium-induced MMP-9 expression and calcium crystal deposition. These studies suggested that the ROS/NF-κB/MMP-9 pathway is having a role in the regulation of calcium crystal deposition in renal tubule [25]. However, MMP-2 is also associated with a higher risk for stones in the patients [52]. MMP-9 and MMP-2 are reported to protect the kidneys from infection, fibrosis, cancer, and injury caused by kidney stones and fibrosis [52–57]. In different studies, it was found that kidney stones may occur in 3%-6% of patients suffering from fibrosis, and kidney stone can precipitate the fibrosis as well [58, 59]. It has been reported that these MMPs are found to be involved in tubular repair after acute kidney injury in renal tubules. These MMPs are found to have a protective effects on kidney diseases (also in urolithiasis[34]). These proteins (MMP2 and 9) are not directly involved in kidney stone formation. However, these are protecting the kidney from deposition of calcium, injury, infection, cancer, and angiogenesis, and fibrosis [25, 52–57, 60]. This means, that if the kidney is protected from stone formation then the kidney can be prevented from injury, fibrosis, and cancer, or angiogenesis/metastasis in the kidney. Targeting these proteins (MMP2 and 9) may be helpful in the management of kidney stones and subsequent morbidities. Nirala et al. targeted these proteins for computational studies to predict binding modes of phytochemical botulin [34].

All the aforementioned proteins were found to have an important role in the management of kidney stones and associated injuries. Therefore, these proteins were selected in these studies to check the binding potential of the phytochemicals of the aerial parts of the *Heliotropium indicum L.*.

The plants possess multiple constituents that work synergistically with minimum side effects and are accessible to a large population. Therefore, natural products have been attractive for drug design and discovery. Various plants like *Aervajavanica, Asparagus racemosus, Curcuma longa, Citrus medica* [3], *Desmodium microphyllum, Eupatorium birmanicum* [10], *Fructus aurantia* [61], *Holarrhenaantidysenterica* [62], *Hordeum vulgare* [63], etc. have been reported in management and treatment of urolithiasis. But still, there is no potential treatment for this disease and people are adopting the surgery to remove stones from the body.

Traditionally, *Heliotropium indicum* L. has been reported to have antioxidant potential [64], prevent stone formation, and bear protective effects to prevent kidney cell damage [65–68]. In the Philippines and Senegal, this plant is used for its diuretic and anti-urolithiasis activity [67, 69, 70]. But there are no reports available about which phytochemicals are responsible for anti-urolithiatic activity from this plant.

Virtual screening is found to be important in the identification of hits/leads against the biological targets in computer-aided drug design and discovery as it is saving time and money [71]. Molecular docking is one of the virtual screening methods which is extensively used for this purpose. This strategy has successfully found the active molecules against the different targets. The molecular docking method is also used to predict binding modes of a ligand inside the active site of the protein and gives docking score [72–74]. Moreover, molecular dynamic simulation (MDS) is also found more important to understand the molecular interactions and binding free energy in presence of water (as a real biological system) at atom level. The MDS is helped a lot to validate and predict the binding affinity and stability of the binding poses obtained from docking studies [75–79]. Therefore, molecular docking and MDS would be useful to identify the potential phytochemicals of *Heliotropium indicum* L. aerial parts against targets for urolithiasis.

In the current studies, multitargets-based virtual screening of phytochemicals found in aerial parts of *Heliotropium indicum* L. was performed against the different biological targets (mentioned above) which were found to be important in the management of kidney stone formation or urolithiasis. For virtual screening, the molecular docking studies were carried out to predict their binding potential against the glycolate oxidase, glutathione-disulfide reductase, glutathione-S-transferase, superoxide dismutase, glutathione peroxidase, Human calcium-sensing receptor, and MMP-9 and MMP-2. This is the first kind of report of individual phytochemicals of *Heliotropium indicum* L. aerial parts that were investigated against multiple targets responsible for urolithiasis or kidney stone. The results indicated that some of the phytochemicals were found to have high binding potential against the targets selected for studies.

2. Methods

2.1 Data set Collection

Data sets of 40 phytochemicals (listed in **Table S1 in supplementary material**), present in the aerial part of *Heliotropium indicum* L. were collected from Google Scholar [66, 67, 69, 80–83]. All the phytochemicals were prepared using LigPrep (Schrödinger LLC) program using the OPLS_2005 force field. All the parameters (including ionization state at pH 7.4, 32 stereoisomers per ligand, retain specified chiralities, desalination, etc.) [Schrödinger Suite 2017: LigPrep, version 2.5, Schrödinger, LLC; New York, USA] were kept as default.

2.2 Multi-targets Virtual Screening

2.2.1 Molecular docking

Total 7 different protein targets, which were found to be responsible for urolithiasis, were downloaded from protein data bank (PDB) [glutathione-disulphide reductase (PDB ID: 1BWC), glutathione-S-transferase(PDB ID:4MPG), superoxide dismutase (PDB ID: 1CB4), glycolate oxidase (PDB ID: 2RDT), MMP-9 (PDB ID: 4XCT), MMP-2 (PDB ID: 1HOV)human calcium-sensing receptor with bound Gd^{3+}(PDB ID: 5FBH), glutathione peroxidase (PDB ID: 2WGR)]for molecular docking based screening. All the protein targets were prepared using the protein preparation wizard from the Maestro program incorporated in Schrödinger (water molecules were removed and hydrogen and missing atoms were also added) software. The receptor grid generation program of the Glide module of the Schrödinger software was used to generate the grid around the active site of the protein. For grid generation, grid size 10X10X10Å was set and center of the grid was selected based on a bound co-crystalized ligand of the PDB. Moreover, the maximum length of docking ligands was set to cut off 20 Å. The grid files are a pre-requisite for molecular docking studies in the Glide program and are important for accurate scoring of docking poses. To validate the docking protocol, first, redock the co-crystalized ligand of the PDB against the active site of the same PDB structure to check whether its binding pose is similar to its experimentally derived pose or not (in terms of position and interactions). In the case of the superoxide dismutase (PDB 1CB4), no co-crystalized ligand was present in the PDB, so a grid was generated around the important residues responsible for the binding of the ligand [84]. The glide docking protocol was repeated three times using different options high-throughput virtual screening (HTVS), standard precision (SP), and extra precision (XP). The accuracy of the docking is increased from HTVS to XP with increased computational time. Each level is filtered out the best binding pose with improved binding affinity. The final refined results will be again subjected to rescoring each XP binding pose in the glide program without docking into the active site [85, 86]. The final results are the best binding pose of each phytochemical against the targets. This protocol was repeated for all protein targets used for the studies.

After successful validation, all the phytochemicals (40 phytochemicals listed in **Table S1 in supplementary material**) were docked into the active site of each target protein using the same grid file. All the docking results were interpreted using the binding pose of the co-crystalized ligand (X-ray) as well as based on available works of literature.

2.3 Validation of docking results

The best binding poses (protein-ligand complexes) were further processed by using the convolutional neural network (CNN) method implemented in Glimpse [87, 88] to predict their binding pose and their affinities. This method was used to validate the binding affinities of the best docking poses of phytochemicals obtained from the Glide program. This prediction will be helpful in the analysis of the final results and of course, to distinguish the high and low binder. If both binding poses, as well as affinities, are consistent, then the docked phytochemical is a high binder against the given protein target.

2.4 Pharmacokinetic studies using QikProp

The pharmacokinetic studies [Absorption, Distribution, Metabolism, and Excretion (ADME)] were evaluated from the QikProp Tool of the Schrödinger program [*QikProp, Schrödinger, LLC, New York, NY, 2020*]. QikProp has predicted the ADME properties from the 95% marketed drugs and provides the ranges of these properties for the predicted molecules. The prediction of the property falls under the range of the QikProp, which means that satisfactory ADME property.

2.5 Molecular dynamic simulation

The molecular dynamic studies were performed using Desmond software [89] provided by D. E. Shaw group [Desmond Molecular Dynamics System, version 2022.1, D. E. Shaw Research, New York, NY]. All the phytochemicals complexes with protein targets were processed for system building (using water and ions) and then generated input files for final dynamic run till 50ns. All the parameters were kept default. All the results were analysed in Maestro and processed further for MM-GBSA calculations in Schrödinger Prime for checking strength of binding affinity.

3. Results

3.1 Docking studies

During the validation of the docking protocol for each target, it was found that the co-crystalized ligand was posed in the same position in the active site as well as exhibited important interactions with active site residues (Table 1). After that, multi-targets based virtual screening was performed using molecular docking studies of the phytochemicals (40 phytochemicals listed in **Table S1 in supplementary material**) present in the leaves of the *Heliotropium indicum L.* against all the selected targets (MMP-9 and MMP-2, glycolate oxidase and human calcium-sensing receptor and antioxidant proteins) with same. The analysis of the docking results was done using the binding pose of the co-crystalized ligand (X-ray) of the target as well as works of literature. Only those poses were selected that were positioned near the co-crystalized ligand of the protein and had the docking score close to the co-crystallized ligand. In the case of superoxide dismutase (PDB ID: 1CB4), the bound co-crystallized ligand is absent, so the cut-off value for docking score > -5.00 kcal/mol was used to select the final pose of the phytochemicals (**Table S2 in supplementary material**).

Table 1

Multitargets based binding interactions analysis of best phytochemicals present in the leaves of *Heliotropium indicum* L. obtained from docking studies

PDB ID	Phytochemicals/ co–crystalized ligand	Docking Score (kcal/mol)	H-bonding	Hydrophobic Interactions
1BWC (Glutathione-disulfide reductase)	*1BWC-X-ray ligand	-11.232	Gly31, Glu50, Ser51, Thr57, Lys66, Ala130, Asp331, Thr339	Ile26, Val49, Cys58, Cys63, Ala130, Phe181, Tyr197, Ile198, Leu298, Ala155, Met202, Val332, Leu337, Leu338, Pro340, Ala342, Phe372
	Pestalamide B	-6.06	Gly31, Thr57, Asp331	Ile26, Val49, Cys58, Ala130, Ala155, Leu298, Ala312
	Rapanone	-5.872	Thr57, Cys58, Asp331	Cys58, Ala155, Tyr197, Ile198, Ala199, Ala288, Val332, Leu337, Leu338, Ala342
	Echinatine	-5.138	Lys66	Cys58, Val61, Gly62, Cys63, Ile198, Tyr197, Leu337, Leu338, Pro340, Val370, Val371, Phe372
	Supinine	-5.038	Leu337, Asp331	Cys58, Val61, Gly62, Cys63, Phe181, Tyr197, Ile198, Met202, Leu337, Leu338, Ala342
4MPG (Glutathione-S-transferase)	*4MPG-x-ray ligand	-5.958	-	Val10, Leu35, Leu114, Leu119 π-π stacking: Trp115
	Pestalamide B	-9.29	Gln12, Gln175, Arg239, Arg242	Val10, Leu35, Val36, Leu114, Trp115, Leu119, Pro228, Ala232, Ala235, Met236 π-π stacking: Trp115
	Rapanone	-8.741	Ser11, Leu54	Val10, Pro13, Leu35, Val36, Leu54, Leu114, Trp115, Leu119, Ala232, Ala235, Met236
	9,12-Octadecadienoic acid	-7.955	Gly111, Trp115, Gln175	Val10, Val35, Val36, Leu54, Ile112, Leu114, Trp15, Leu119, Ala232, Ala235, Met236
	Lasiocarpine	-7.454	His40	Val10, Leu35, Val36, Leu54, Ile112, Leu114, Trp115, Leu119, Ile216, Ala235, Met236
	3`-Acetyllycopsamine	-7.262	Gln12, His40, Leu54, Arg107	Val10, Pro13, Leu35, Val36, Leu54, Leu114, Trp115, Leu119, Ala232, Ala235, Met236
	Trachelanthamine	-7.238	Gln12, His40, Arg107, Trp115	Val10, Leu119, Pro13, Leu35, Leu114, Trp115, Ala232, Ala235, Met236,
	Lycopsamine	-7.017	His40, Leu54, Arg107	Pro13, Leu35, Val36, Leu54, Trp115, Leu119, Ala232, Ala235, Met236
	Supinine	-6.750	Gln12, Arg107	Val10, Pro13, Leu35, Val36, Leu114, Trp115, Leu119, Ala232, Ala235, Met236
	9,12,15-Octadecatrienoic acid, Ethyl Ester	-6.711	Gln175	Val10, Leu35, Val36, Leu54, Leu114, Trp115, Leu119, Ala232, Ala235, Met236
	Acetyl indicine	-6.507	Gln12, Arg107	Val10, Pro13, Leu35, Val36, Leu54, Leu114, Trp115, Leu119, Ala232, Ala235, Met236
	Heleurine	-6.404	Gln12, Arg107	Val10, Pro13, Leu35, Val36, Ile112, Leu114, Trp115, Leu119, Ala232, Ala235, Met236
	Campesterol	-6.021	-	Val10, Pro13, Leu35, Val36, Leu114, Trp115, Leu119, Ile216, Pro228, Ala232, Ala235, Met236
	Heliotrine	-5.965	His40	Val10, Leu35, Val36, Leu54, Leu114, Trp115, Leu119, Ala235, Met236
1CB4 (Superoxide dismutase)	Rinderine	-6.597	Val7, Val146	Val5, Cys6, Val7, Leu8, Cys144, Val146, Ile147,
	Lycopsamine	-6.594	Val7, Val146	Val5, Cys6, Val7, Leu8, Cys144, Val146, Ile147
	Heliotrine	-6.232	Val7, Asn51, Val146	Cys6, Val7, Leu8, Cyc55, Cys144, Val146,
	Supinine	-5.788	Val7, Val146	Val5, Cys6, Val7, Cys144, Val146, Ile147
	Acetyl indicine	-5.537	Val7, Val146	Val5, Cys6, Val7, Leu8, Cys144, Val146, Ile147
	Echinatine	-5.493	Val7, Val146	Val5, Cys6, Val7, Leu8, Cys144, Val146, Ile147
	Trachelanthamine	-5.453	Val7, Val146	Val5, Cys6, Val7, Leu8, Cys144, Val146, Ile147, Ile149
	Pestalamide B	-5.396	Val7, Asn51, Val146	Val5, Cys6, Val7, Cys55, Cys144, Val146, Ile147

*binding interactions were obtained from Plip program also [Adasme, M. F. et al. PLIP 2021: expanding the scope of the protein–ligand interaction profiler to DNA and RNA. Nucl. Acids Res. (2021). doi: 10.1093/nar/gkab294]

PDB ID	Phytochemicals/ co–crystalized ligand	Docking Score (kcal/mol)	H-bonding	Hydrophobic Interactions
2RDT (Glycolate oxidase)	2RDT-x-ray ligand	-8.505	Arg167, Arg263	Tyr26, Ala81, Met82, Trp110, Tyr132, Leu164, Leu205, Tyr208, Val209
	Pestalamide B	-11.597	Ala79, Ala81, Arg167, Cys236, His260 Arg263	Tyr26, Ala79, Ala81, Met82, Trp110, Tyr132, Leu164, Leu205, Tyr208, Val209
	Rapanone	-10.606	Tyr26, Ala79, Tyr132, Arg167, Arg263	Tyr26, Ala79, Ala81, Met82, Trp110, Ala111, Tyr132, Leu164, Leu205, Tyr208, Val209
	Supinine	-8.252	Tyr26, Arg167, His260, Arg263	Tyr26, Ala81, Met82, Tyr132, Trp110, Leu164, Leu205, Tyr208, Val209
	Rinderine	-7.826	Tyr26, Ala81, Arg167	Tyr26, Ala79, Ala81, Met82, Trp110, Tyr132, Leu164, Leu205, Val209, Ile213
4XCT (Matrix metalloproteinase-9)	4XCT-X-ray-ligand	-5.916	Leu188, Ala189	Leu187, Leu188, Ala189, Ala191, Leu222, Val223, Leu243, Tyr245, Pro246, Met247, Tyr248 **Cation-pi**: with Zn^{2+} π-π stacking: His226
	3`-Acetyllycopsamine	-8.778	Pro240, Arg249	Leu188, Leu222, Val223, Pro240, Ala242, Leu243, Tyr245, Pro246, Met247, Tyr248, Pro255
	Lycopsamine	-8.502	Ala242, Arg249	Leu188, Val223, Leu222, Pro240, Ala242, Leu243, Pro255, Tyr248, Met247, Pro246, Tyr245, Tyr248, Met244, Pro246, Ala189
	Pestalamide B	-7.747	Leu188, Ala189, Tyr245	Leu222, Val223, Leu187, Leu188, Ala189, Pro240, Ala242, Leu243, Tyr245, Pro246, Met247, Tyr248 π-π stacking: **His226**
	Rinderine	-7.683	Tyr245 Glu227	Leu187, Leu188, Ala189, Leu222, Val223, Pro240, Ala242, Leu243, Tyr245, Pro246, Met244, Tyr248
	Rapanone	-7.401	Ala189	Leu187, Leu188, Ala189, Leu222, Val223, Pro240, Ala242, Leu243, Tyr245, Pro246, Met247, Tyr248, Phe250
	Echinatine	-7.302	Met247, Arg249	Leu187, Leu188, Ala189, Leu222, Val223, Ala242, Leu243, Tyr245, Pro246, Met247, Tyr248
	Heliotrine	-7.214	Glu227	Leu187, Leu188, Ala189, Ala191, Leu222, Val223, Ala242, Leu243, Tyr245, Pro246, Met247, Tyr248
	Dodecanoic acid	-7.059	Ala189	Leu187, Leu188, Ala189, Leu222, Val223, Ala242, Leu243, Tyr245, Met247, Tyr248, Pro255
	Homo spermidine	-7.053	Ala189, Glu227, Try245, Arg249	Leu188, Ala189, Leu222, Val223, Leu243, Tyr245, Pro246, Met247, Tyr248, Phe250
	Acetyl indicine	-6.929	Met247, Arg249	Leu187, Leu188, Ala189, Leu222, Val223, Ala242, Leu243, Tyr245, Pro246, Met247, Tyr248
	Supinine	-6.683	Glu227	Leu187, Leu188, Ala189, Leu222, Val223, Ala242, Leu243, Tyr245, Pro246, Met247, Tyr248
	Heleurine	-6.582	Glu227	Phe181, Leu187, Leu188, Ala189, Leu222, Val223, Ala242, Leu243, Tyr245, Pro246, Met247, Tyr248, Pro255
	Trachelanthamine	-6.329	Glu227	Leu187, Leu188, Ala189, Leu222, Val223, Ala242, Leu243, Met244, Tyr245, Pro246, Met247, Tyr248
	9,12-Octadecadienoic acid	-6.231	Glu227	Leu187, Leu188, Ala189, Leu222, Val223, Ala242, Leu243, Met244, Tyr245, Pro246, Met247, Tyr248
	Tetradecanoic acid	-6.037	Glu227	Leu188, Ala189, Leu222, Val223, Ala242, Leu243, Tyr245, Pro246, Met247, Tyr248, Phe250, Pro255
5FBH (Human calcium sensing receptor)	*5FBH-X-ray-ligand	-6.241	Ser147, Ala168, Ser170, Glu297	Thr145, Ala298 π-π stacking: Trp70

*binding interactions were obtained from Plip program also [Adasme, M. F. et al. PLIP 2021: expanding the scope of the protein–ligand interaction profiler to DNA and RNA. Nucl. Acids Res. (2021). doi: 10.1093/nar/gkab294]

PDB ID	Phytochemicals/ co–crystalized ligand	Docking Score (kcal/mol)	H-bonding	Hydrophobic Interactions
	3`-Acetyllycopsamine	-8.725	Ser147, Ala298	Pro39, Phe42, Trp70, Ala168, Tyr218, Pro274, Ala298, Trp299, Leu304, Ile416
	Echinatine	-8.227	Asp275, Ala298	Pro39, Phe42, Trp70, Tyr218, Pro274, Ala298, Trp299, Leu304, Ile416,
	Acetyl indicine	-8.133	Arg66, Ala168, Ala298	Pro39, Phe42, Trp70, Ala168, Ile187, Tyr218, Pro274, Ala298, Trp299, Leu304, Ile416
	Rinderine	-8.122	Ala298	Pro39, Phe42, Trp70, Ala168, Tyr218, Pro274, Ala298, Trp299, Leu304, Ile416
	Supinine	-8.003	Ala298	Pro39, Phe42, Trp70, Ala168, Tyr218, Pro274, Ala298, Trp299, Leu304, Ile416
	Lycopsamine	-7.904	Ala168, Ala298	Pro39, Phe42, Trp70, Ala168, Ile187, Tyr218, Pro274, Ala298, Trp299, Ile416
	Rapanone	-7.311	Asn64, Ala298	Pro39, Phe42, Trp70, Ala168, Tyr218, Pro274, Ala298, Trp299, Ile416
	Heliotrine	-6.965	Ala298	Pro39, Phe42, Trp70, Ala168, Tyr218, Pro274, Ala298, Trp299, Leu304
	Heleurine	-6.961	Ala298	Pro39, Phe42, Trp70, Ala168, Tyr218, Pro274, Ala298, Trp299, Leu304, Ile416
	Lasiocarpine	-6.465	Asn102, Ser272	Pro39, Phe42, Trp70, Val104, Val149, Ala168, Ile187, Tyr246, Pro274, Ala298, Ile416
	Trachelanthamine	-6.365	Ala168	Pro39, Phe42, Trp70, Ala168, Ile187, Tyr218, Pro274, Ala298, Trp299, Leu322, Leu304, Ile416
2WGR (Glutathione peroxidase)	*2WGR-X-ray-ligand	-9.512	Thr125, Lys131, Trp132, Tyr149	*Salt bridge: Lys131, Arg148
	Lycopsamine	-5.648	Gln122, His123, Arg148,	Pro151, Tyr149
	Rinderine	-5.395	His123, Thr125	Pro151, Tyr149
1HOV (Matrix metalloproteinase-2)	1HOV-X-ray-lig	-12.375	Leu83, Ala84, Ile141	Tyr74, Leu82, Leu83, Ala84, Leu116, Ala136, Leu137, Ala139, Pro140, Ile141, Tyr142, Tyr144, Phe148 Cation pi: Zn^{2+}
	Lasiocarpine	-6.962	Leu83, Ala84, Tyr142	Leu82, Leu83, Ala84, Tyr112, Val117, Ala139, Pro140, Ile141, Tyr142
	3`-Acetyllycopsamine	-6.503	Leu83, Ala84, His85, Glu121	Leu82, Leu83, Ala84, Ala86, Val117, Tyr142
	Supinine	-6.415	Leu83, Ala84, Glu121	Leu82, Leu83, Ala84, Ala86, Phe87, Tyr142
	Rinderine	-6.319	Leu83, Ala84, Glu121	Leu82, Leu83, Ala84, Ala86, Val117, Ala139, Pro140, Ile141, Tyr142
	Pestalamide B	-6.24	Leu83, Ala84,	Leu82, Leu83, Ala84, Leu116, Val117, Ala136, Leu137, Ala139, Ile141, Tyr142, Tyr144, Leu150
	Lycopsamine	-6.234	Glyu81, Leu83, Ala84, Glu121	Leu82, Leu83, Ala84, Ala86, Ala139, Pro140, Ile141, Tyr142
	5-Hydroxymethylfurfural	-5.439	Leu83, Ala84, Ala139	Leu82, Leu83, Ala84, Val117, Met138, Ala139, Pro140, Ile141, Tyr142 Cation-pi: Zn Pi-pi: His120
	Rapanone	-5.432	Leu83, Glu121	Leu82, Leu83, Tyr112, Val117, Ala84, Ala139, Pro140, Ile141, Tyr142
	Heliotrine	-5.405	Leu83, Ala84, Glu121	Leu82, Leu83, Ala84, Ala86, Leu116, Val117, Pro140, Ile141, Tyr142
	Echinatine	-5.374	Ala84, Glu121	Leu82, Leu83, Ala84, Ala86, Val117, Ala139, Pro140, Ile141, Tyr142

*binding interactions were obtained from Plip program also [Adasme, M. F. et al. PLIP 2021: expanding the scope of the protein–ligand interaction profiler to DNA and RNA. Nucl. Acids Res. (2021). doi: 10.1093/nar/gkab294]

PDB ID	Phytochemicals/ co–crystalized ligand	Docking Score (kcal/mol)	H-bonding	Hydrophobic Interactions
	Tetradecanoic acid	-5.262	Ala84	Leu82, Leu83, Ala84, Tyr74, Pro75, Phe76
	Trachelanthamine	-5.256	Leu83, Ala84	Leu82, Leu83, Ala84, Ala139, Pro140, Ile141, Tyr142
	1-Hexacosanol	-5.241	Leu83, Ala84	Leu82, Leu83, Ala84, Tyr112, Val117, Ala139, Pro140, Ile141, Tyr142, Tyr144
	Campesterol	-5.151	Ile141	Tyr74, Leu82, Leu83, Ala84, Ala139, Pro140, Ile141, Tyr142
	Phenol, 3-Isopropoxy-5-Methyl	-5.005	Ala136	Ile116, Pro134, Ala136, Leu137, Ala139, Ile141, Tyr142, Tyr144, Phe148

*binding interactions were obtained from Plip program also [Adasme, M. F. et al. PLIP 2021: expanding the scope of the protein–ligand interaction profiler to DNA and RNA. Nucl. Acids Res. (2021). doi: 10.1093/nar/gkab294]

The docking results (Table 1) against glutathione-disulfide reductase (PDB ID: 1BWC), elucidated that pestalamide B (**Fig. 1a**), rapanone (**Fig. 2a**), echinatine (**Fig. S1**), and supinine (**Fig. 3a**) bound into the active site at the same position where co-crystallized ligand posed. However, these phytochemicals were found to have low binding potential as compared to co-crystallized ligands (-11.232 kcal/mol). The rest of the molecules were found to have less docking scores as compared to Supinine (-5.038 kcal/mol) [**Table S2 in supplementary material**]. The 2D docking poses of the pestalamide B, rapanone, echinatine, and supinine are given in **Fig. S2, S3, S4**, and **S5**, respectively. The important H-bonding interactions were observed with the Gly31, Thr57 Lys66, and Asp331 residues while, Ile26, Val49, Cys58, Cys63, Ala130, Ala155, Tyr197, Ile198, Leu298, Val332, Leu337, Leu338, and Ala342 residues were involved in hydrophobic interactions (Table 1).

The docking results (Table 1) against glutathione-S-transferase (PDB ID:4MPG), elucidated that out of the 40 phytochemicals, 17 phytochemicals (**Table S2 in supplementary material**) were found to a have higher binding affinity for co-crystallized ligand (-5.96 kcal/mol). However, pestalamide B (-9.29 kcal/mol) (**Fig. 1b and S6**) and rapanone (-8.741 kcal/mol) (**Fig. 2b and S7**) were found to have the highest docking score as compared to co-crystallized ligand (Table 1). The pestalamide B (pyridine-4(1H)-one ring) exhibited pi-pi interactions with Trp115 similar to the co-crystallized ligand (**Fig. S6** and **S8**, respectively). The rest of the phytochemicals also exhibited high docking scores (ranging from − 5.965 to -7.955 kcal/mol) as compared to the co-crystalized ligand (Table 1). The phytochemicals [pestalamide B, rapanone, 9,12-octadecadienoic acid, lasiocarpine, 3`-acetyllycopsamine, trachelanthamine, lycopsamine, supinine,9,12,15-octadecatrienoic acid, ethyl ester, acetyl indicine, heleurine, campesterol, heliotrine] had the highest binding affinities against the glutathione-S-transferase (Table 1). The important H-bonding interactions (with Gln12, His40, Leu54, Arg107, Trp115, Gln175) and hydrophobic interactions (with Val10, Pro13, Leu35, Val36, Leu54, Leu114, Trp115, Leu119, Ala235, Ala232, and Met236) were observed with the 13 phytochemicals (Table 1). The rest of the molecules exhibited less binding affinity (less docking score) as compared to the co-crystallized ligand (**Table S2 in supplementary material**).

The docking studies against superoxide dismutase (PDB ID: 1CB4) revealed that rinderine (-6.597 kcal/mol), lycopsamine (-6.594 kcal/mol) and heliotrine (-6.232 kcal/mol) were exhibiting the highest docking score (Table 1 **and Fig. S9-S11, respectively**). However, supinine (-5.788 kcal/mol) (**Fig. 3c and S12**), acetyl indicine (-5.537 kcal/mol) (**Fig. S13**), echinatine (-5.493 kcal/mol) (**Fig. S14**), trachelanthamine (-5.453 kcal/mol) (**Fig. S15**), pestalamide B (-5.396kcal/mol) (**Fig. 1c and S16**) also exhibited high binding affinities against the superoxide dismutase. All the phytochemicals (Table 1) were docked at the same position in the protein active site as well as reflected the almost same H-bonding and hydrophobic interactions (Table 1). The rest of the molecules exhibited less docking score than the cut-off value of -5.00 kcal/mol [**Table S2 in supplementary material**]. All phytochemicals (**in** Table 1) followed the same binding interaction as H-bonding (Val7 and Val146) and hydrophobic interactions (Val5, Cys6, Val7, Leu8, Cys144, Val146, Ile147). This suggests that these interactions were found to be important for binding the molecules into the active site of the protein. The rinderine, lycopsamine, heliotrine, supinine, acetyl indicine, echinatine, trachelanthamine, pestalamide B were found to have high binding potential against the superoxide dismutase.

The docking results (Table 1) against glycolate oxidase (PDB ID: 2RDT) elucidated that pestalamide B (-11.597 kcal/mol) (**Fig. 1d and S17**), rapanone (-10.606kcal/mol)(**Fig. 2c and S18**) have the highest docking score as compared to co-crystallized ligand (-8.505 kcal/mol) (**Fig. S19 in supplementary material)**. In addition, supinine (-8.252 kcal/mol) (**Fig. 3d and S20 in supplementary material**) exhibited almost the same binding affinity as a co-crystalized ligand (Table 1). The rest of the phytochemicals (Table 1) were having less binding affinity as compared to a co-crystalized ligand. The important H-bonding (Tyr26, Ala79, Tyr132, Arg167, His260, andArg263) and hydrophobic interactions (Tyr26, Ala81, Met82, Trp110, Tyr132, Leu164, Leu205, Tyr208, Val209) were found with these phytochemicals. However, some of the phytochemicals exhibited common binding interactions either H-boding/hydrophobic interactions or both (as reflected in Table 1). The rest of the phytochemicals exhibited less docking score (<-5.00 kcal/mol), thereby, these were not included for analysis (**Table S2 in supplementary material**).

The docking results of MMP-9 (PDB ID: 4XCT) showed that a total of 15 phytochemicals out of 40 exhibited a high docking score as compared to co-crystallized ligand (Range − 6.037 to -8.778 kcal/mol) (Table 1). The 3`-acetyllycopsamine (-8.778kcal/mol) (**Fig. S21**) and lycopsamine (-8.502 kcal/mol) (**Fig. S22**) showed the highest docking score as compared to co-crystallized ligand (-5.916 kcal/mol) (**Fig. S23 in supplementary material)**. On the other hand, the phytochemicals like pestalamide B (-7.747 kcal/mol) (**Fig. 1e and S24)** rinderine (-7.683 kcal/mol) (**Fig. S25**), rapanone (-7.401 kcal/mol) (**Fig. 2d and S26**) also exhibited a good binding affinity against MMP-9 as compared to the co-crystalized ligand. The π-π stacking interactions with His226 were also observed in pestalamide B (**Fig. S24**) as similar to the co-crystallized ligand (Table 1). The important H-bonding (Ala189, Leu188, Glu227, Pro240, Met247, Arg249) and hydrophobic interactions (Leu188, Val223, Leu222, Pro240, Ala242, Leu243, Tyr245, Pro246, Met247, Tyr248, Pro255) were observed with the

top 15 phytochemicals. The rest of the phytochemicals exhibited less binding affinity as compared to the co-crystallized ligands (**Table S2 in Supplementary material**).

The docking results (Table 1) of the human calcium-sensing receptor (PDB ID: 5FBH) elucidated that 11 out of 40 phytochemicals were found to have a good binding affinity (from – 6.365 to -8.725 kcal/mol) as compared to co-crystallized ligand (-6.241 kcal/mol). All of these phytochemicals were docked into the same active site where the co-crystalized ligand was bound. Highest binding affinity (above >-8.00 kcal/mol) was exhibited by the phytochemicals; 3`-acetyllycopsamine (-8.725 kcal/mol) (**Fig. S27**), echinatine (-8.227 kcal/mol) (**Fig. S28**), Acetyl indicine (-8.133 kcal/mol) (**Fig. S29)**, rinderine (-8.122 kcal/mol) (**Fig. S30**), Supinine (-8.003 kcal/mol) (**Fig. 3f and S31**). On the other hand, phytochemicals lycopsamine (-7.904 kcal/mol), rapanone (-7.311 kcal/mol) (**Fig. 2e**), heliotrine (-6.965 kcal/mol), heleurine (-6.961 kcal/mol), lasiocarpine (-6.465 kcal/mol) and trachelanthamine (-6.365 kcal/mol) also exhibited the high binding affinity against human calcium-sensing receptor. All these phytochemicals exhibited the common H-bonding interactions with Ala298, except lasiocarpine and Trachelanthamine (Table 1). This signifies that it could be an important interaction for binding the molecules into the active site of the human calcium-sensing receptor (PDB: 5FBH). However, other H-bonding interactions with Ser147, and Ala168were also observed with the phytochemicals (Table 1). The important hydrophobic (Trp70, Pro39, Phe42, Ala168, Tyr218, Pro274, Ala298, Trp299, Leu304, Ile416) interactions were observed in top-ranked phytochemicals (Table 1). The remaining phytochemicals were also found to bind with active sites but with less binding affinity as compared to that of co-crystalized ligand (**Table S2 in supplementary material**).

The docking studies against glutathione peroxidase (PDB ID: 2WGR) observed that all the phytochemicals exhibited a less binding affinity with active sites of the glutathione peroxidase as compared to co-crystallized ligand (-9.512 kcal/mol) (Table 1 and **Table S2 in supplementary material)**. The lycopsamine (-5.648 kcal/mol) and rinderine (-5.395 kcal/mol) exhibited a good docking score as compared to other phytochemicals, but lower than the co-crystalized ligand (Table 1 and **Table S2 in supplementary material**). The H-bonding interactions Arg148, His123 Gln122 in the case of lycopsamine and Thr125, His123 in the case of rinderine were observed. Both the phytochemicals showed hydrophobic interactions with the residues Pro151, Tyr149.These phytochemicals exhibited a low binding affinity as the binding pocket of the PDB ID 2WGR is too small to accommodate them. Because of it, only small size phytochemicals were able to bind into the active site with less binding affinity as compared to the co-crystallized ligand (Fig. 10 and **Table S2**). So, these phytochemicals were found to have less binding potential against glutathione peroxidase, however, this is important antioxidant protein target.

The docking studies of all the phytochemicals against MMP-2 (PDB ID: 1HOV) exhibited a low docking score as compared to co-crystallized ligand (-12.375 kcal/mol) (Table 1 and **Table S2 in supplementary material**). However, these phytochemicals were docked at the same position (where co-crystallized ligand was bound) and with common H-bonding (Leu83, Ala84, Glu121) and hydrophobic (Leu82, Leu83, Ala84, Ala86, Val117, Ala139, Pro140, Ile141, Tyr142) interactions (Table 1). These phytochemicals were found to have less binding potential against MMP-2 as compared to the co-crystalized ligand.

By comparing the overall docking results (Table 1), it is found that the phytochemicals: pestalamide B, rapanone, supinine, were found to be the best-docked phytochemicals against the different targets used in the studies (minimum 5 protein targets, Table 1) and possess higher binding affinity towards selected targets. However, secondly, 9,12-Octadecadienoic acid, lasiocarpine, 3`-acetyllycopsamine, trachelanthamine, lycopsamine, heliotrine, rinderine, echinatine, dodecanoic acid, homo spermidine, acetyl indicine, heleurine, 5-hydroxymethylfurfural, tetradecanoicacid, 1-hexacosanol, campesterol, and Phenol-3-isopropoxy-5-methyl were also found best docked phytochemicals against the different protein targets used in the studies (minimum two proteins, Table 1) and possess higher binding affinity towards selected targets. However, the rest of the phytochemicals were not found to exhibit good binding poses into the active site of either of the targets used in the studies or were docked with a less binding affinity (Table 1 and S2 **in supplementary material**). These results suggested that these phytochemicals may have anti-urolithiasis activity. Figure 4 represented the 2D structure of the phytochemicals used for docking validation purposes.

Table 2
Binding affinities of each phytochemical obtained from multitargets based virtual screening using docking methods in Glide and Glimpse (give in bracket) programs for anti-urolithiatic activity

	Docking Score kcal/mol (*dG (kcal/mol)							
PDB ID	**4MPG**	**1CB4**	**2RDT**	**1BWC**	**2WGR**	**1HOV**	**4XCT**	**5FBH**
Phytochemicals								
X-ray ligands	-5.958 (-5.2567)	-	-8.505 (-7.744)	-11.232 (-9.102)	-9.512 (-6.411)	-12.375 (-11.108)	-5.916 (-11.145)	-6.241 (-8.003)
Pestalamide B	-9.295 (-8.223)	-5.396 (-4.348)	-11.597 (-7.384)	-6.06 (-8.362)	-	-6.24 (-8.228)	-7.747 (-9.687)	-5.813 (-7.925)
Rapanone	-8.741 (-9.283)	-	-10.606 (-10.881)	-5.872 (-7.631)	-	-5.432 (-11.369)	-7.401 (-10.697)	-7.311 (-8.385)
9,12-Octadecadienoic acid	-7.955 (-8.319)	-	-	-	-		-6.231 (-8.941)	-
Lasiocarpine	-7.454 (-9.148)	-	-	-	-	-6.962 (-9.602)	-	-6.465 (-8.487)
3`-Acetyllycopsamine	-7.262 (-8.468)	-	-	-	-	-6.503 (-8.836)	-8.778 (-10.689)	-8.725 (-7.524)
Trachelanthamine	-7.238 (-7.857)	-5.453 (-5.672)	-	-	-	-5.256 (-7.419)	-6.329 (-10.397)	-6.365 (-7.474)
Lycopsamine	-7.017 (-7.739)	-6.594 (-5.28)	-	-	-5.648 (-6.749)	-6.234 (-7.926)	-8.502 (-9.982)	-7.904 (-7.856)
Heliotrine	-5.965 (-7.849)	-6.232 (-5.767)	-	-	-	-5.405 (-8.140)	-7.214 (-10.269)	-6.965 (-7.198)
Supinine	-6.75 (-8.413)	-5.788 (-5.792)	-8.252 (-10.631)	-5.038 (-7.681)	-	-6.415 (-8.464)	-6.683 (-10.321)	-8.003 (-7.701)
Rinderine	-	-6.597 (-5.052)	-	-	-5.395 (-5.998)	-6.319 (-8.052)	-7.683 (-10.034)	-8.122 (-7.820)
Echinatine	-	-5.493 (-5.899)	-	-5.138 (-6.495)	-	-5.374 (-7.811)	-7.302 (-9.233)	-8.227 (-7.295)
Dodecanoic acid	-	-	-	-	-	-	-7.059 (-8.0278)	-
Homo spermidine	-	-	-	-	-	-	-7.053 (-7.593)	-
Acetyl indicine	-6.507 (-8.927)	-5.537 (-6.369)	-	-	-	-	-6.929 (-10.102)	-8.133 (-7.381)
Heleurine	-6.404 (-8.536)	-	-	-	-	-	-6.582 (-10.199)	-6.961 (-7.088)
5-Hydroxymethylfurfural	-	-	-	-	-	-5.439 (-5.472)	-	-
Tetradecanoic_acid	-	-	-	-	-	-5.262 (-10.571)	-6.037 (-8.123)	-
1-Hexacosanol	-	-	-	-	-	-5.241	-	-

*calculated from Glimpse tool [53]; Glutathione-disulfide reductase (PDB ID: 1BWC), Glutathione-S-transferase (PDB ID:4MPG), Superoxide dismutase (PDB ID: 1CB4), Glycolate oxidase (PDBID: 2RDT), Glutathione peroxidase (PDB ID: 2WGR), Matrix metalloproteinase-9 (PDB ID: 4XCT), Matrix metalloproteinase-2 (PDB 1HOV), Human calcium sensing receptor (PDB ID: 5FBH)

	Docking Score kcal/mol (*dG (kcal/mol)							
PDB ID Phytochemicals	4MPG	1CB4	2RDT	1BWC	2WGR	1HOV	4XCT	5FBH
						(-8.804)		
Campesterol	-6.021 (-10.817)	-	-	-	-	-5.151 (-0.087)	-	-
Phenol_3-Isopropoxy-5-Methyl	-	-	-	-	-	-5.005 (-4.259)	-	-
9,12,15-Octadecatrienoic acid ethyl ester	-6.711 (-9.888)	-	-	-	-	-	-	-
Helindicine	-	-	-	-	-	-	-	-5.202 (-5.692)

*calculated from Glimpse tool [53]; Glutathione-disulfide reductase (PDB ID: 1BWC), Glutathione-S-transferase (PDB ID:4MPG), Superoxide dismutase (PDB ID: 1CB4), Glycolate oxidase (PDBID: 2RDT), Glutathione peroxidase (PDB ID: 2WGR), Matrix metalloproteinase-9 (PDB ID: 4XCT), Matrix metalloproteinase-2 (PDB 1HOV), Human calcium sensing receptor (PDB ID: 5FBH)

3.2 Validation of docking results

All the best-docked phytochemicals were subjected for validation of binding poses as well as affinities obtained from the GLIDE program using CNN method implemented in Glimpse tool. These prediction results suggested that the phytochemicals exhibited satisfactory binding affinities (Table 2) and generated almost the same binding poses as found in the Glide program. The best docked molecules in the both program (glide for docking and scoring and Glimpse for prediction of binding affinity) were pestalamide B, Rapanone, Supinine. These results reflected that generated binding poses from different tools were found to have consistency in docking results (with binding poses and affinities Tables 1 and 2). Hence, validation of all the docking results were successfully established using another docking tool: Glimpse. Table 2 is showing the binding affinities of each phytochemical obtained from multitargets-based virtual screening using docking methods in Glide and Glimpse (give in bracket) programs for anti-urolithiasis activity.

3.3 Pharmacokinetic studies using QikProp

The ADME studies of the 40 molecules were evaluated from the QikProp of the Schrodinger program. **Table S3** is given the details of the pharmacokinetic studies. From these studies, it was reflected that all the phytochemicals exhibited a satisfactory ADME profile.

3.4 Molecular dynamic simulations

The MDS studies were performed only for best docking poses of the phytochemicals: pestalamide B, rapanone and supinine against all the given targets in Table 2. The MDS was performed till 50ns in Desmond 2022 program. The results were analysed for stability of the phytochemicals into the active site of the targets during the course of the MDS by using RMSD value. The RMSD was calculated for backbone atoms of the complexes with respect to docked structure. Next, binding free energies for all the complexes were also calculated to check the binding affinity against the each anti-urolithiatic target. For this purpose, last 10ns or 200 frames were used as convergence was observed (Fig. 4a-4h) during this time scale.

Upon binding of the phytochemicals: pestalamide B, rapanone, supinine with protein targets (given in Table 2), all the proteins were almost found stable (< 1 Å RMSD fluctuations) in last 200 frames of MDS (Fig. 4a-4h), except glutathione-disulfide reductase (Fig. 4a for supinine and X-ray-lig-FAD), matrix metalloproteinase-2 (Fig. 4c for supinine), glycolate oxidase (Fig. d for rapanone), glutathione peroxidase (Fig. 4e for pestalamide B), and glutathione-S-transferase, matrix metalloproteinase-9, human calcium sensing receptor (Fig. 4f, 4g, and 4h for supinine, respectively) as found > 1 Å RMSD fluctuations.

In case supinine complexes with the targets, some of the protein targets were found stable (< 1 Å RMSD fluctuations) such as glycolate oxidase (Fig. 4d) and glutathione peroxidase (Fig. 4e). This means no significance conformational changes was found upon binding of the supinine with these targets. The supinine was unstable as leave the active site of superoxide dismutase (Fig. 4b) in last 10ns of simulation time. Therefore, it was not included in the analysis.

In the case of complexes with rapanone, glutathione-disulfide reductase (Fig. 4a), matrix metalloproteinase-2 (Fig. 4c), glutathione peroxidase (Fig. 4e), glutathione-S-transferase (Fig. 4f), matrix metalloproteinase-9 (Fig. 4g) and human calcium sensing (Fig. 4h) targets were found stable and had < 1 Å RMSD fluctuations. The most importantly all the proteins were found stable upon binding of Pestalamide B (Fig. 4a-4h). When Pestalamide B was binding with these targets, then protein got stabilized and had < 1 Å RMSD fluctuations. The overall RMSD fluctuations analysis of protein-phytochemical complexes, it was found that the phytochemicals: rapanone and pestalamide B were contributed a lot in stability of the protein targets upon binding as compared to supinine (Fig. 4a-4h).

The intermolecular H-bonding interactions were also calculated during the course of MDS to measure the frequencies as well as strength of H-bonding of the phytochemical against the different protein targets used here. It was found that Pestalamide-B [Glu50 (80%), Thr57 (110%),, Arg291 (70%), Asp331 (140%)] and Rapanone [Ser30 (80%), Gly55 (55%), Cys58 (90%), Asp331 (65%), Ala336 (70%)] were exhibited the strong H-bonding with Glutathione-disulfide reductase (PDB ID: 1BWC). During the simulation, some of the residues were exhibited the more 100% contribution in H-boding means these residues were

made multiple H-bonding contacts with the ligand. However, Supinine was having low H-bonding via residue Gly62 (35%). The Pestalamide-B had very low H-bonding frequencies against superoxide dismutase (PDB ID: 1CB4) during the simulation with different residues including Asn51 (27%) and Asn63 (22%).

The H-bonding interactions with the Matrix metalloproteinase-2 (PDB ID: 1HOV) by Pestalamide-B [Leu83 (90%), Ala84 (60%), Glu121 (96%), Ala136 (80%)] were higher as compared to Rapanone [Gly81 (50%) Thr106 (48%),] during simulation. However, supinine was exhibited the H-bonding interactions with residues Leu83 (70%) and Ala84 (27%).

In case of Glycolate oxidase (PDB ID: 2RDT), Pestalamide-B [Arg167 (50%), Lys236 (80%), Arg263 (223%), and Asp291 (90%)] and Supinine [Tyr26 (62%), Gly165 (23%), Phe175 (32%), Gln264 (80%)] was having high H-boding interactions. However, and Rapanone [Tyr163 (18%), Arg263 (15%), Gln264 (17%)] were exhibited the low H-bonding interactions during the complete simulation time.

The low to moderate H-bonding interactions with the Glutathione peroxidase (PDB ID: 2WGR) were exhibited by Rapanone [Ala45 (27%), Asn107 (18%), Pro151 (25%)] and Pestalamide-B [Thr125 (40%) and Arg148 (50%),], respectively. However, supinine were had very less (< 1%) H-bonding interactions during the simulation time.

The pestalamide-B and rapanone were had high H-boding interactions with Trp115 (100%) and Leu54 (100%), respectively against glutathione-S-transferase (PDB ID: 4MPG). But pestalamide-B exhibited the low H-bonding interactions with Arg239 (20%). On the other hand, supinine were shown the H-boding interactions with the Ser11 (70%), Gln12 (40%) and His40 (23%).

In case of the Matrix metalloproteinase-9 (PDB ID: 4XCT), PestalamideB was exhibited the strong H-bonding interactions with the Glu227 (90%) during the simulation. In addition, this phytochemical was also involved in the strong ionic interactions (100%) with the His226, His230 and His236 during MDS. In case of the Rapanone, 100% ionic interactions were found with the residues His226, Glu227, His230 and His236. These interactions were involved to make PestalamideB and Rapanone stable during the MDS. The supinine was having low interactions against Matrix metalloproteinase-9 during the simulation.

While interacting with the Human calcium sensing receptor (PDB ID: 5FBH), all the three phytochemicals: Pestalamide-B [Ser147 (250%), Ser170 (80%), Ser272 (90%)], Rapanone [Asn64(110%), Ala298 (70%)] and Supinine [Asn64 (50%), Arg66 (100%)] were exhibited the strong H-bonding interactions during the MDS.

In addition to the H-bonding interactions, hydrophobic and water bridging interactions were also observed with the phytochemicals against the protein targets. But H-boding interactions was having upper hand as compared to other interactions.

Over all H-bonding analysis reflected that Pestalamide-B and Rapanone were exhibited highest H-bonding frequencies during the simulation time as compared to supinine.

To check the binding affinities of all the three phytochemicals (pestalamide B, Rapanone, Supinine) against each protein target, all the complexes were processed for binding free energy calculations via MM/GBSA calculations in Prime tool of Schrödinger package.

For Pestalamide B, binding free energy was found higher against the 6 different protein targets such as glutathione-S-transferase (-56.185 kcal/mol), glycolate oxidase (-60.358 kcal/mol), matrix metalloproteinase-2 (-69.176 kcal/mol), matrix metalloproteinase-9 (-46.205 kcal/mol), human calcium sensing receptor (-70.320 kcal/mol) and glutathione peroxidase (-32.424 kcal/mol) as compared to co-crystallized ligands (-38.229 kcal/mol, -55.612 kcal/mol, -66.922 kcal/mol, -31.193 kcal/mol, -30.544 kcal/mol, -25.976 kcal/mol, respectively). However, less binding free energy against glutathione-disulfide reductase (-47.372 kcal/mol) and superoxide dismutase (-22.732 kcal/mol) targets were observed.

The rapanone was also found high binding free energy against the 4 protein targets only [glutathione-S-transferase (-51.002 kcal/mol), matrix metalloproteinase-9 (-35.757 kcal/mol), human calcium sensing receptor (-57.831 kcal/mol), and glutathione peroxidase (-37.999 kcal/mol)] as compared to co-crystallized ligands (given above). However, rest of the complexes [Glycolate oxidase (-49.516 kcal/mol), matrix metalloproteinase-2 (-57.942 kcal/mol), glutathione-disulfide reductase (-58.191 kcal/mol)] with rapanone were exhibited the lower binding free energy.

Similarly, supinine were exhibited the high binding free energy with 4 different targets (different from the case of rapanone) [glutathione-S-transferase (-50.680 kcal/mol), glycolate oxidase (-55.028 kcal/mol), matrix metalloproteinase-9 (-38.338 kcal/mol), human calcium sensing receptor (-39.908 kcal/mol)] as compared to co-crystallized ligands (given above).

Overall binding free energy analysis, it was found that pestalamide-B was found to be very good binder against most of the protein targets used for anti-urolithiatic studies. But, rapanone and supinine was ranked second as only exhibited good binding affinity against 4 anti-urolithiatic protein targets and this energy is low as compared to pestalamide-B.

4. Discussion

Currently, phytochemicals are being explored for their medicinal properties and are attaining a lot of attention in drug discovery. Phytochemicals have diversified biological activities and are traditionally used as folk medicine in varieties of diseases[90, 91]. Therefore, ethnopharmacological studies of phytochemicals still need scientific attention to reveal the pharmacological effects of the phytochemicals in the body i.e. identification of signalling pathways or proteins which are responsible for therapeutic action [92]. In the field of computer-aided drug design, the molecular docking technique constantly holds great attention. It is a powerful tool to explore new phytochemical binding potential against the receptors/proteins of well-known structures. Hence, it plays an important part to identify the therapeutic targets for the phytochemicals [93–95].

Traditionally, the *Heliotropium indicum* L. plant is helpful in the prevention of urolithiasis[67–69]. There is no existing data available that identifies specific phytochemicals in the leaves responsible for anti-urolithiasis activity. Therefore, multi targets based virtual screening studies were designed to understand the binding potential of the different phytochemicals found in the *Heliotropium indicum* L. leaves, against different protein targets responsible for urolithiasis.

The results of the docking studies reflected that only three phytochemicals: pestalamide B, rapanone, and supinine exhibited the highest binding modes with almost all the protein targets used in the studies except glutathione peroxidase (an antioxidant target).These phytochemicals interacted with the protein targets which are responsible for kidney stone formation such as glycolate oxidase, MMP-9, MMP-2, and human calcium-sensing receptor (Tables 1 and 2). These phytochemicals exhibited computationally good binding affinities as well as characteristics of binding interactions, therefore, these may have high propensity to show anti-urolithiasis effects (Table 2 and **Fig. 1, 2, and 3**).

In addition, 3
$-acetyllycopsa\ \min e, trachelantha\ \min e, lycopsa\ \min e, heliotr \in e, r \in der \in e,\ \text{ and } e\chi nat \in ehavealsoexhibitedhighb \in d \in g\ \mathrm{m}$
-acetyllycopsamine for glutathione-S-transferase, trachelanthamine, lycopsamine, and heliotrine for glutathione-S-transferase and superoxide dismutase, rinderine for superoxide dismutase and glutathione peroxidase, Echinatine for superoxide dismutase and glutathione-disulfide reductase (Tables 1 and 2). It is reflected that these phytochemicals also exhibited satisfactory binding modes with the used protein targets.

Some of the phytochemicals: lasiocarpine, acetyl indicine, and heleurine exhibited good binding modes against MMP-2 or 9 and human calcium-sensing receptors along with an antioxidant target: glutathione-S-transferase only. However, acetyl indicine was also found to have binding modes with superoxide dismutase. These molecules were reported to have binding potential against the important targets of urolithiasis, but not against all the selected targets in the studies (Tables 1 and2).

The 9,12-Octadecadienoic acid, 5-hydroxymethylfurfural, tetradecanoicacid, 1-Hexacosanol, campesterol, Phenol-3-Isopropoxy-5-methylexhibited the binding modes against MMP 2 or/and 9 targets (Table 2). However, tetradecanoic acid also exhibited the binding modes against MMP9. The 9, 12-octadecadienoic acid, and campesterol also exhibited the binding modes against an antioxidant target: glutathione-S-transferase. The remaining best-docked phytochemicals like 9, 12, 15-Octadecatrienoic acid ethyl ester, and helindicine only docked into the active site of glutathione-S-transferase and human calcium-sensing receptors, respectively.

The ADME studies of the best-selected phytochemicals (pestalamide B, rapanone, supinine, 3`-acetyl lycopsamine, trachelanthamine, lycopsamine, heliotrine, rinderine, and echinatine) from docking studies exhibited the prediction within the recommended range of the ADME prediction (**Table S3**). This means, that all these phytochemicals are having a drug-like properties as well as good pharmacokinetic profiles.

Overall binding mode analysis reflected that the pestalamide B, rapanone, and supinine were found with best binding modes in docking studies against all the anti-urolithiatic targets. In addition,3`-acetyl lycopsamine, trachelanthamine, lycopsamine, heliotrine, rinderine, echinatine (Fig. 4) were also posed satisfactory, but with some anti-urolithiasis targets (MMP-2 or MMP-9 and human calcium-sensing receptors) only and all the antioxidant targets. All these phytochemicals (pestalamide B, rapanone, supinine, 3`-Acetyl lycopsamine, trachelanthamine, lycopsamine, heliotrine, rinderine, echinatine) have been explored first time in kidney stone or urolithiasis. All these phytochemicals exhibited a satisfactory ADME profile in pharmacokinetic studies.

The MDS studies were also performed to validate the best docking results (pestalamide B, rapanone, and supinine) in term of stability of the complexes into the active site as well as strength of the binding against all the targets used in the studies. It was found that pestalamide B was performed best in the MDS studies as RMSD fluctuation of protein targets were less than 1 Å (in bound state), strong H-boding and high bind free energy with all the proteins (as discussed in results section). Such consistency was not followed by rapanone in term of binding free energy only with the targets. It had high binding free energy in case of four protein targets only (as discussed in the MDS section), but it was found low as compared to pestalamide B. The supinine were also had higher binding free energy as compared to co-crystallized ligands in case of four protein targets only (as discussed in MDS results section). These three phytochemicals (pestalamide B, rapanone, supinine) were exhibited the high binding potential against anti-oxidant as well as anti-urolithiatic targets. The evidence from the literatures [30–33, 40, 41], the antioxidant activities of the phytochemicals are beneficial in the prevention of urolithiasis/kidney stone. Therefore, the high antioxidant potential of these phytochemicals computationally may also support here to enhance the therapeutic effects in the management of urolithiasis/kidney stones. The rest of the phytochemicals were found to have binding modes with few antioxidants and either MMP-2 or 9 and human calcium-sensing receptors. For confirmation of the anti-urolithiatic potency of the individual phytochemicals, experimental studies need to be performed. Due to structural diversity among the phytochemicals, docking results exhibited diversity in the binding affinities as well as in the binding modes.

5. Conclusions

Multi-targets-based virtual screening is an effective approach to depict the binding modes of the different phytochemicals against the active site of multiple targets using molecular docking methods. The docking studies of the phytochemicals of the *Heliotropium indicum L.* leaves elucidated that the phytochemicals like pestalamide B, rapanone, and supinine generated excellent results in terms of binding modes and affinities against anti-urolithiasis as well as antioxidant targets. The complexes of these phytochemicals were further validated in MDS studies. It was found that pestalamide-B was performed excellent binding with the different protein targets in MDS studies in term of stability of the proteins, binding interactions and binding free energy. However, rapanone was satisfactorily good as compared to supinine. The multi-targeted in-silico screening identified that these phytochemicals (pestalamide-B > rapanone > Supinine) had high antioxidant as well as anti-urolithiatic binding properties and may play an important role in the management of urolithiasis or kidney stone. However, further experimental verifications are warranted. This could be the possible reason why *Heliotropium indicum* L. plant was used in urolithiasis or kidney stone. These computational results can be advantageous to identify similar or design more novel phytochemicals /chemicals against urolithiasis or kidney stone.

Declarations

Competing Interest: No competing interests

Ethics approval and consent to participate: Not applicable

Consent for publication: Not applicable.

Availability of data and material: Not available to others

Funding: Not applicable

Authors' contributions

Mr. Vivek, and Dr. Pawan made the concept of the paper. Dr. Pawan executed, analyse the results and wrote the complete manuscript. Dr. Anju and Dr. Vishnu edit and updated the manuscript. All authors read and approved the final manuscript

Acknowledgements:

Dr. Pawan Gupta are very thankful to the DST-SERB for providing the TARE grant from 2019-22 (Ref. No.: TAR/2019/260). Dr. Pawan Gupta acknowledges the D. E. Shaw group, USA for providing Desmond 2022.1 software [Desmond Molecular Dynamics System, version 2022.1, D. E. Shaw Research, New York, NY].

References

1. Touhami M, Laroubi A, Elhabazi K et al (2007) Lemon juice has protective activity in a rat urolithiasis model. BMC Urol 7(1):1–10
2. Anbu J, Suman S, SLVVSN KSK, Kumar RS, Nithya S, Kannadhasan R (2011) Antiurolithiatic activity of ethyl acetate root extract of Ichnocarpus frutescens using ethylene glycol induced method in rats. J Pharm Sci Res 3(4):1182
3. Tiwari A, Soni V, Londhe V, Bhandarkar A, Bandawane D, Nipate S (2012) An overview on potent indigenous herbs for urinary tract infirmity: urolithiasis. Asian J Pharm Clin Res 5(1):7–12
4. Atodariya U, Barad R, Upadhyay S, Upadhyay U (2013) Anti-urolithiatic activity of Dolichos biflorus seeds. J Pharmacogn Phytochem 2 (2)
5. Yadav RD, Jain S, Alok S, Mahor A, Bharti JP, Jaiswal M (2011) Herbal plants used in the treatment of urolithiasis: a review. Int J Pharm Sci Res 2(6):1412–1420
6. Shirfule AL, Racharla V, Qadri S, Khandare AL (2013) Exploring antiurolithic effects of gokshuradi polyherbal ayurvedic formulation in ethylene-glycol-induced urolithic rats. Evid Based Complement Alternat Med 2013
7. Baker PW, Coyle P, Bais R, Rofe AM (1993) Influence of season, age, and sex on renal stone formation in South Australia. Med J Aust 159(6):390–392
8. Devi VK, Baskar R, Varalakshmi P (1993) Biochemical effects in normal and stone forming rats treated with the ripe kernel juice of Plantain (Musa Paradisiaca). Anc Sci Life 12(3–4):451
9. Heller HJ, Sakhaee K, Moe OW, Pak CY (2002) Etiological role of estrogen status in renal stone formation. J Urol 168(5):1923–1927
10. Mikawlrawng K, Kumar S, Vandana R (2014) Current scenario of urolithiasis and the use of medicinal plants as antiurolithiatic agents in Manipur (North East India): a review. Int J Herb Med 2(1):1–12
11. Kumar S, Kumar K, Srinivasa V, Bilal S (2012) A review on urolithiasis. Int J Univers Pharm Life Sci 2(2):269–280
12. Khan SR, Kok DJ (2004) Modulators of urinary stone formation. Front Biosci 9(629):1450–1482
13. Basavaraj DR, Biyani CS, Browning AJ, Cartledge JJ (2007) The role of urinary kidney stone inhibitors and promoters in the pathogenesis of calcium containing renal stones. EAU-EBU update Ser 5(3):126–136
14. Aggarwal KP, Narula S, Kakkar M, Tandon C (2013) Nephrolithiasis: molecular mechanism of renal stone formation and the critical role played by modulators. BioMed Res Int 2013
15. Chhiber N, Sharma M, Kaur T, Singla S (2014) Mineralization in health and mechanism of kidney stone formation. Int J Pharm Sci Invent 3:25–31
16. Barbas C, Garcıa A, Saavedra L, Muros M (2002) Urinary analysis of nephrolithiasis markers. J Chromatogr B 781(1–2):433–455
17. Coe FL, Evan A, Worcester E (2005) Kidney stone disease. J Clin Invest 115(10):2598–2608
18. Bensatal A, Ouahrani M (2008) Inhibition of crystallization of calcium oxalate by the extraction of Tamarix gallica L. Urol Res 36(6):283–287
19. Miano R, Germani S, Vespasiani G (2007) Stones and urinary tract infections. Urol Int 79(Suppl 1):32–36
20. KVSRG P, Sujatha D, Bharathi K (2007) Herbal drugs in urolithiasis-a review. Pharmacogn Rev 1(1):175–178
21. Butterweck V, Khan SR (2009) Herbal medicines in the management of urolithiasis: alternative or complementary? Planta Med 75(10):1095–1103
22. Khan SR (2014) Reactive oxygen species, inflammation and calcium oxalate nephrolithiasis. Translational Androl Urol 3(3):256
23. Khan SR (2013) Reactive oxygen species as the molecular modulators of calcium oxalate kidney stone formation: evidence from clinical and experimental investigations. J Urol 189(3):803–811
24. Boonla C (2018) Oxidative Stress in Urolithiasis. Reactive Oxygen Species (ROS) in Living Cells; InTech: London, UK:129 – 59
25. Wu Y, Zhang J, Li C et al (2021) The Activation of ROS/NF-κB/MMP-9 Pathway Promotes Calcium-Induced Kidney Crystal Deposition. Oxid Med Cell Longevity 2021. (Article ID 8836355) https://doi.org/10.1155/2021/8836355

26. Huang H-S, Chen J, Chen C-F, Ma M-C (2006) Vitamin E attenuates crystal formation in rat kidneys: roles of renal tubular cell death and crystallization inhibitors. Kidney Int 70(4):699–710
27. Naghii MR, Eskandari E, Mofid M, Jafari M, Asadi MH (2014) Antioxidant therapy prevents ethylene glycol-induced renal calcium oxalate crystal deposition in Wistar rats. Int Urol Nephrol 46(6):1231–1238
28. Morgan MS, Pearle MS (2016) Medical management of renal stones. BMJ 352
29. Baia LC, Baxmann AC, Moreira SR, Holmes RP, Heilberg IP (2012) Noncitrus alkaline fruit: a dietary alternative for the treatment of hypocitraturic stone formers. J Endourol 26(9):1221–1226
30. Marhoume FZ, Aboufatima R, Zaid Y et al (2021) Antioxidant and Polyphenol-Rich Ethanolic Extract of Rubia tinctorum L. Prevents Urolithiasis in an Ethylene Glycol Experimental Model in Rats. Molecules 26(4):1005
31. Naghii M, Eskandari EM, Jafari M, Asadi M M (2014) Antioxidant therapy prevents ethylene glycol-induced renal calcium oxalate crystal deposition in Wistar rats. Int Urol Nephrol 46(6):1231–1238
32. Saha S, Shrivastav P, Verma R (2014) Antioxidative mechanism involved in the preventive efficacy of Bergenia ciliata rhizomes against experimental nephrolithiasis in rats. Pharm Biol 52(6):712–722
33. Ghulam MS, Muhammad S, Urooj M et al (2021) Herbal remedies used for the management of urolithiasis in Abbottabad, Northern Pakistan. Plant Sci Today 8(4):836–847
34. Nirala RK, Dutta P, Malik MZ, Dwivedi L, Shrivastav TG, Thakur SC (2019) In Vitro and In Silico Evaluation of Betulin on Calcium Oxalate Crystal Formation. J Am Coll Nutr 38(7):586–596. 10.1080/07315724.2019.1568321
35. Shirfule AL, Sangamwar AT, Khobragade CN (2011) Exploring glycolate oxidase (GOX) as an antiurolithic drug target: Molecular modeling and in vitro inhibitor study. Int J Biol Macromol 49(1):62–70. https://doi.org/10.1016/j.ijbiomac.2011.03.016
36. Murray MS, Holmes RP, Lowther WT (2008) Active Site and Loop 4 Movements within Human Glycolate Oxidase: Implications for Substrate Specificity and Drug Design. Biochemistry 47(8):2439–2449. 10.1021/bi701710r
37. Fargue S (2019) Metabolism of Glycolate to Oxalate in Kidney Proximal Tubule Cells. FASEB J 33(S1):8637–8637
38. Martin-Higueras C, Luis-Lima S, Salido E (2016) Glycolate oxidase is a safe and efficient target for substrate reduction therapy in a mouse model of primary hyperoxaluria type I. Mol Ther 24(4):719–725
39. Wang M, Xu M, Long Y et al (2016) High throughput cell-based assay for identification of glycolate oxidase inhibitors as a potential treatment for Primary Hyperoxaluria Type 1. Sci Rep 6(1):1–12
40. Selvam R (2002) Calcium oxalate stone disease: role of lipid peroxidation and antioxidants. Urol Res 30(1):35–47. 10.1007/s00240-001-0228-z
41. Azimi A, Eidi A, Mortazavi P, Rohani AH (2021) Protective effect of apigenin on ethylene glycol-induced urolithiasis via attenuating oxidative stress and inflammatory parameters in adult male Wistar rats. Life Sci 279:119641
42. Gallwitz H, Bonse S, Martinez-Cruz A, Schlichting I, Schumacher K, Krauth-Siegel RL (1999) Ajoene Is an Inhibitor and Subversive Substrate of Human Glutathione Reductase and Trypanosoma cruzi Trypanothione Reductase: Crystallographic, Kinetic, and Spectroscopic Studies. J Med Chem 42(3):364–372. 10.1021/jm980471k
43. Hough MA, Hasnain SS Crystallographic structures of bovine copper-zinc superoxide dismutase reveal asymmetry in two subunits: functionally important three and five coordinate copper sites captured in the same crystal11Edited by, Huber R (1999) J Mol Biol 287 (3):579 – 92. https://doi.org/10.1006/jmbi.1999.2610
44. Dimastrogiovanni D, Anselmi M, Miele AE et al (2010) Combining crystallography and molecular dynamics: The case of Schistosoma mansoni phospholipid glutathione peroxidase. Proteins Struct Funct Bioinf 78(2):259–270. https://doi.org/10.1002/prot.22536
45. Zhang C, Zhang T, Zou J et al (2016) Structural basis for regulation of human calcium-sensing receptor by magnesium ions and an unexpected tryptophan derivative co-agonist. Sci Adv 2(5):e1600241. 10.1126/sciadv.1600241
46. Evan AE, Lingeman JE, Coe FL et al (2008) Histopathology and surgical anatomy of patients with primary hyperparathyroidism and calcium phosphate stones. Kidney Int 74(2):223–229. 10.1038/ki.2008.161
47. Vezzoli G, Terranegra A, Rainone F et al (2011) Calcium-sensing receptor and calcium kidney stones. J Transl Med 9(1):201. 10.1186/1479-5876-9-201
48. Renkema KY, Bindels RJM, Hoenderop JGJ (2011) Role of the Calcium-Sensing Receptor in Reducing the Risk for Calcium Stones. Clin J Am Soc Nephrol 6(8):2076–2082. 10.2215/cjn.00480111
49. Nuti E, Cantelmo AR, Gallo C et al (2015) N-O-Isopropyl Sulfonamido-Based Hydroxamates as Matrix Metalloproteinase Inhibitors: Hit Selection and in Vivo Antiangiogenic Activity. J Med Chem 58(18):7224–7240. 10.1021/acs.jmedchem.5b00367
50. Feng Y, Likos JJ, Zhu L et al (2002) Solution structure and backbone dynamics of the catalytic domain of matrix metalloproteinase-2 complexed with a hydroxamic acid inhibitor. Biochim Biophys Acta Proteins Proteom 1598(1):10–23. https://doi.org/10.1016/S0167-4838(02)00307-2
51. Narula S, Tandon C, Tandon S (2018) Role of matrix metalloproteinases in degenerative kidney disorders. Curr Med Chem 25(15):1805–1816
52. Sharma KL, Misra S, Kumar A, Mittal B (2012) Higher risk of matrix metalloproteinase (MMP-2, 7, 9) and tissue inhibitor of metalloproteinase (TIMP-2) genetic variants to gallbladder cancer. Liver Int 32(8):1278–1286
53. Cheng Z, Limbu MH, Wang Z et al (2017) MMP-2 and 9 in Chronic Kidney Disease. Int J Mol Sci 18(4):776
54. Chuang H-M, Chen Y-S, Harn H-J (2019) The Versatile Role of Matrix Metalloproteinase for the Diverse Results of Fibrosis Treatment. Molecules 24(22):4188

55. Kaneko T, Shimizu A, Mii A et al (2012) Role of matrix metalloproteinase-2 in recovery after tubular damage in acute kidney injury in mice. Nephron Experimental Nephrol 122(1–2):23–35
56. Xu C, Zhang W, Lu P et al (2021) Mutation of Klotho rs3752472 protect the kidney from the renal epithelial cell injury caused by CaOx crystals through the Wnt/β-catenin signaling pathway. Urolithiasis. 10.1007/s00240-021-01269-z
57. Yoodee S, Noonin C, Sueksakit K et al (2021) Effects of secretome derived from macrophages exposed to calcium oxalate crystals on renal fibroblast activation. Commun Biol 4(1):959. 10.1038/s42003-021-02479-2
58. Liu M, Liu Y-Z, Feng Y et al (2013) Novel evidence demonstrates that epithelial-mesenchymal transition contributes to nephrolithiasis-induced renal fibrosis. J Surg Res 182(1):146–152
59. Plant BJ, Goss CH, Plant WD, Bell SC (2013) Management of comorbidities in older patients with cystic fibrosis. Lancet Respiratory Med 1(2):164–174
60. Okada A, Yasui T, Fujii Y et al (2010) Renal macrophage migration and crystal phagocytosis via inflammatory-related gene expression during kidney stone formation and elimination in mice: Detection by association analysis of stone-related gene expression and microstructural observation. J Bone Miner Res 25(12):2701–2711
61. Li X, Liang Q, Sun Y et al (2015) Potential mechanisms responsible for the antinephrolithic effects of an aqueous extract of Fructus aurantii. Evid Based Complement Alternat Med 2015
62. Khan A, Khan SR, Gilani AH (2012) Studies on the in vitro and in vivo antiurolithic activity of Holarrhena antidysenterica. Urol Res 40(6):671–681
63. Shah JG, Patel BG, Patel SB, Patel RK (2012) Antiurolithiatic and antioxidant activity of Hordeum vulgare seeds on ethylene glycol-induced urolithiasis in rats. Indian J Pharmacol 44(6):672
64. Gopinathan M, Balasubramanian M (2021) correlation analysis of phytochemicals and antioxidant activities of *Heliotropium indicum l.* leaves extracts. Int J Pharm Sci Res 12(8):4386–4396. 10.13040/IJPSR.0975-8232.12
65. Adelaja AA, Ayoola M, Otulana J, Akinola O, Olayiwola A, Ejiwunmi A (2008) Evaluation of the histo-gastroprotective and antimicrobial activities of Heliotropium indicum Linn (Boraginaceae). Malays J Med Sci 15(3):22
66. Ovalle J, Ovalle J, Garcia O (2022) Systematic review of the phytochemical compounds use of Heliotropium indicum taking advantage of its advantage in modern medicine. J Appl Biotechnol Bioeng 9(5):132–136
67. Sarkar C, Mondal M, Khanom B et al (2021) Heliotropium indicum L.: From Farm to a Source of Bioactive Compounds with Therapeutic Activity. Evid Based Complement Alternat Med 2021:9965481
68. Ghosh P, Das P, Das C, Mahapatra S, Chatterjee S (2018) Morphological characteristics and Phyto-pharmacological detailing of Hatishur (Heliotropium indicum Linn.): A concise review. J Pharmacogn Phytochem 7(5):1900–1907
69. Quisumbing E (1951) Medicinal plants of the Philippines. Department of Agriculture and Commerce, Philippine Islands Technical Bulletin (16):1234 pp
70. Berhault J (1974) Floore Illustree du Senegal, Govt. Senegal, Min Rural Development. Water For Div Dakar 2:110–114
71. Singh S, Gupta P, Gupta J (2020) Virtual structural similarity elucidates bioactivity of Fenchone: Enriched phytochemical in fennel essential oil. Curr Drug Discovery Technol 17(5):619–630. 10.2174/1570163816666190321142826
72. Gupta P, Gupta S, Sinha S, Sundaram S, Sharma VK, Munshi A (2023) In silico phytochemical repurposing of natural molecules as entry inhibitors against RBD of the spike protein of SARS-CoV-2 using molecular docking studies. Int J Comput Biol Drug Des 15(4):267–288
73. Ridhwan MJM, Bakar SIA, Latip NA, Ghani NA, Ismail NH (2022) A comprehensive analysis of human CYP3A4 crystal structures as a potential tool for molecular docking-based site of metabolism and enzyme inhibition studies. J Comput Biophys Chem 21(03):259–285
74. Jana P, Bhardwaj B (2021) Exploration of some naturally occurring fungal-derived bioactive molecules as potential SARS-CoV-2 Main Protease (MPro) inhibitors through in-silico approach. J Comput Biophys Chem 20(03):251–266
75. Güven MH, Garip AK (2022) The Candidate Molecules, RBD-ACE2 Binding Inhibitors to Prevent Sars-CoV-2 Infection. J Comput Biophys Chem 21(07):769–781
76. Zheng Z, Jin J, Liu L et al (2022) Understanding the Binding Mode of Losartan Upon GPVI via a Molecular Simulation Study. J Comput Biophys Chem 21(01):23–34
77. Ounissi M, Rachedi FZ (2022) Targeting the SARS-CoV-2 Main Protease: In Silico Study Contributed to Exploring Potential Natural Compounds as Candidate Inhibitors. J Comput Biophys Chem 21(06):663–682
78. Taslimi P, Erden Y, Mamedov S et al (2021) The biological activities, molecular docking studies, and anticancer effects of 1-arylsuphonylpyrazole derivatives. J Biomol Struct Dyn 39(9):3336–3346
79. Saini G, Dalal V, Gupta DN, Sharma N, Kumar P, Sharma AK (2021) A molecular docking and dynamic approach to screen inhibitors against ZnuA1 of Candidatus Liberibacter asiaticus. Mol Simul :1–16
80. Ramamurthy V, Nethaji S, Rajakumar R (2014) Determination of the therapeutic Compounds and Antimicrobial activity of Heliotropium indicum By GC/MS. Glo J Biol Agricul Health Sci 3(3):261–264
81. Fayed MA (2021) Heliotropium; a genus rich in pyrrolizidine alkaloids: A systematic review following its phytochemistry and pharmacology. Phytomedicine Plus 1(2):100036
82. Yeo D, Attioua B, Lehalle C et al (2011) Isolation of wound healing compounds from Heliotropium indicum. J Appl Pharm Sci (Issue) :102–106
83. Dash G, Abdullah M (2013) A review on Heliotropium indicum L.(Boraginaceae). Int J Pharm Sci Res 4(4):1253
84. Pandey P, Ahmed B, Khan HA, Bala M, Prasad J (2019) In silico molecular docking and comparative in-vitro analysis of ethyl 3, 4, 5-trihydroxybenzoate and its derivative isolated from Hippophae rhamnoides leaves as free radical scavenger and anti-inflammatory compound. Pharmacognosy Magazine

15(64):313

85. Friesner RA, Murphy RB, Repasky MP et al (2006) Extra Precision Glide: Docking and Scoring Incorporating a Model of Hydrophobic Enclosure for Protein – Ligand Complexes. J Med Chem 49(21):6177–6196. 10.1021/jm051256o
86. Raj U, Varadwaj PK (2016) Flavonoids as Multi-target Inhibitors for Proteins Associated with Ebola Virus: In Silico Discovery Using Virtual Screening and Molecular Docking Studies. Interdisciplinary Sciences: Comput Life Sci 8(2):132–141. 10.1007/s12539-015-0109-8
87. Jiménez J, Škalič M, Martínez-Rosell G, De Fabritiis G (2018) KDEEP: Protein–Ligand Absolute Binding Affinity Prediction via 3D-Convolutional Neural Networks. J Chem Inf Model 58(2):287–296. 10.1021/acs.jcim.7b00650
88. Varela-Rial A, Maryanow I, Majewski M et al (2022) PlayMolecule glimpse: Understanding protein–ligand property predictions with interpretable neural networks. J Chem Inf Model 62(2):225–231
89. Bowers KJ, Chow E, Xu H et al (2006) Scalable algorithms for molecular dynamics simulations on commodity clusters. Proceedings of the 2006 ACM/IEEE Conference on Supercomputing p. 84-es
90. Grigalunas M, Burhop A, Christoforow A, Waldmann H (2020) Pseudo-natural products and natural product-inspired methods in chemical biology and drug discovery. Curr Opin Chem Biol 56:111–118. https://doi.org/10.1016/j.cbpa.2019.10.005
91. Chen Y, Kirchmair J (2020) Cheminformatics in Natural Product-based Drug Discovery. Mol Inf 39(12):2000171. https://doi.org/10.1002/minf.202000171
92. Süntar I (2019) Importance of ethnopharmacological studies in drug discovery: role of medicinal plants. Phytochem Rev :1–11
93. Zhang H, Pan J, Wu X, Zuo A-R, Wei Y, Ji Z-L (2019) Large-scale target identification of herbal medicine using a reverse docking approach. ACS Omega 4(6):9710–9719
94. Lee A, Lee K, Kim D (2016) Using reverse docking for target identification and its applications for drug discovery. Expert Opin Drug Discovery 11(7):707–715
95. Katsila T, Spyroulias GA, Patrinos GP, Matsoukas M-T (2016) Computational approaches in target identification and drug discovery. Comput Struct Biotechnol J 14:177–184. https://doi.org/10.1016/j.csbj.2016.04.004

Figures

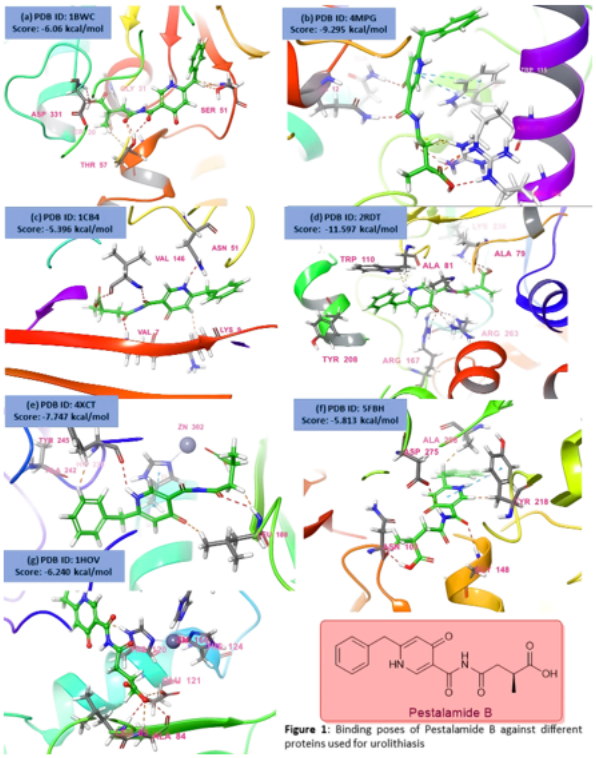

Figure 1

See image above for figure legend.

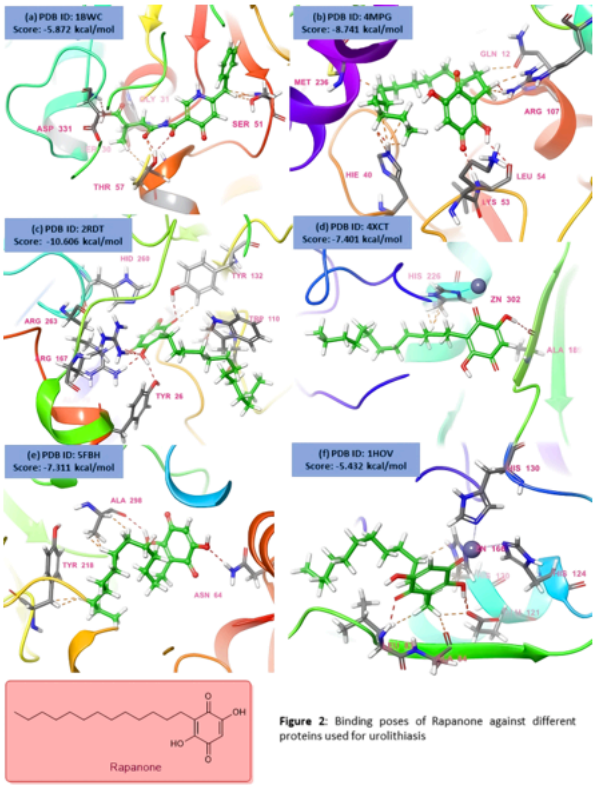

Figure 2

See image above for figure legend.

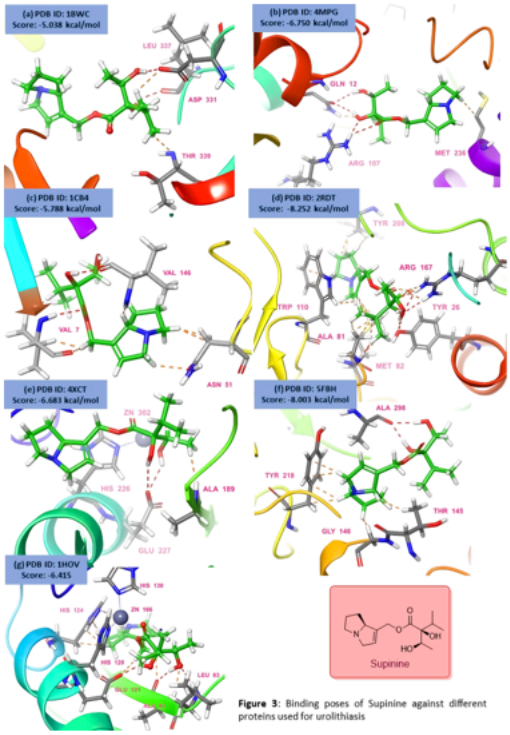

Figure 3

See image above for figure legend.

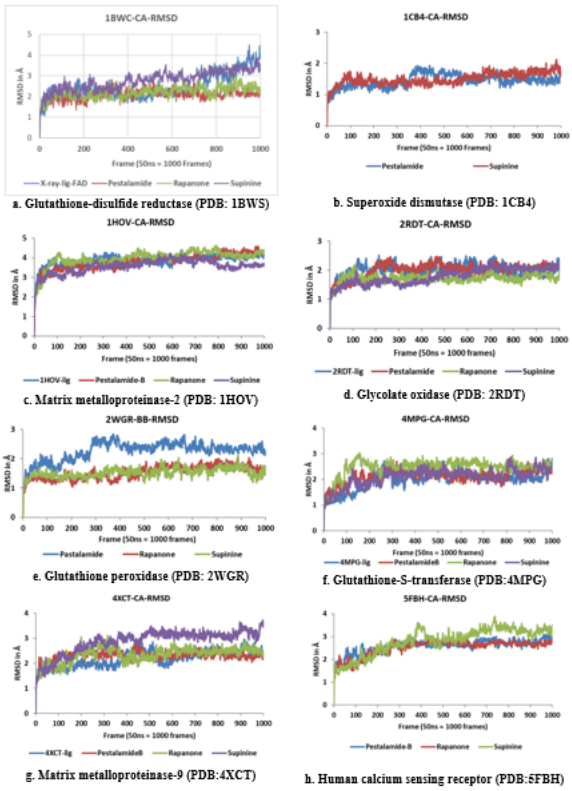

Figure 4

RMSD plots for C-alpha of the protein targets (from a to h) bound with ligands (X-ray ligands, pestalamide, rapanone, and supinine till 50ns MDS

Supplementary Files

This is a list of supplementary files associated with this preprint. Click to download.

- supplementraymaterial.docx